ELECTROMAGNETIC SCATTERING FROM A CIRCULAR TARGET ABOVE OR BELOW ROUGH SURFACE

X. Wang, C.-F. Wang, and Y.-B. Gan

Temasek Laboratories
National University of Singapore
10 Kent Ridge Crescent, Singapore 119260

L.-W. Li

Department of Electrical and Computer Engineering
National University of Singapore
10 Kent Ridge Crescent, Singapore 119260

Abstract—The electromagnetic scattering from a perfectly electric conducting (PEC) target located above or below rough surface is investigated, for the case of TM polarization, using the Method of Moments (MoM). The rough surface with Gaussian profile is used to emulate the realistic situation of a statistically-rough surface, while the tapered incident wave is chosen to reduce the truncation error. The Monte-Carlo procedure is employed to calculate the angular correlation function (ACF), which is dependent on the depth, size and horizontal position of the buried target, as well as the moisture content in the soil, and the properties of the rough surface. The enhancement of the ACF on the non-memory line can be used to detect a target below the rough surface. The analysis on the statistical characteristics is also carried out, in view of the study on target detection.

1. INTRODUCTION

Electromagnetic scattering from rough surface and subsurface targets has been a problem of long-term interest, as the targets above or below the rough surface are affected by the surrounding medium. In many cases, the interface is often considered to be a planar dielectric boundary [1, 2]. However, the contribution from the rough surface can significantly modify the scattering from the target, as compared to that from a flat surface. Some approximate analytical solutions can only be found in the case of small roughness limit [3–7, 21–24]. Numerical simulation of scattering from both target and rough surface is available in the literature [8, 9], which can be used to detect and identify the buried targets, such as mines, pipes, and tunnels [10]. To characterize target below the rough surface, the angular correlation function (ACF) was used to study the scattering from random rough surface. The ACF is the correlation function of two scattered fields in the directions θ_{s1} and θ_{s2}, corresponding to two incident fields in θ_{i1} and θ_{i2}, respectively. It is calculated by taking the average over realization (samples) of different rough surfaces. The ACF of scattered fields from rough surface exhibits a strong correlation known as the angular memory effect, which is generally small away from the memory line [11, 12]. The memory line obeys the angular relation $\sin\theta_{s2} - \sin\theta_{s1} = \sin\theta_{i2} - \sin\theta_{i1}$, which is a consequence of the statistical translation invariance of the random rough surface. The ACF technique has been applied to detect object buried in rough surface. Results show that away from the memory line, the rough surface scattering contribution to ACF is small, and the value of the ACF is completely dominated by the scattering from the buried object.

The ACF technique is superior to the conventional method based on backscattering cross section, for the TE case [13, 14].

In this paper, we investigate the scattering of tapered incident wave from a target above or below the rough surface in the TM case. The solution of the scattered field is obtained by the Method of Moment (MoM). The ACF is investigated as a function of the depth, size and horizontal position of the buried target, as well as the moisture content in the soil and the properties of the rough surface generated using the Monte-Carlo method. The calculation of the ACF shows that the enhancement of the ACF on non-memory line can be used to detect target placed below the rough surface, through appropriate choices of the reference and variable angles. The analysis on the statistical characteristics of the scattered field amplitude from object located above rough surface will also be discussed.

2. DESCRIPTION OF THE STATISTICAL SURFACE

The scattered fields for a single, deterministic rough surface may be useful in some cases, for example, in the comparisons with experimental results for fixed, real surface. In general, one seeks the stochastic scattering properties of an ensemble of surfaces with a given statistical distribution. The random rough surface is often characterized by the surface height probability distribution. The commonly used surface height probability distribution function is the Gaussian distribution. The non-Gaussian surface height profile has been studied and generated using different approaches [15, 16], and finds certain applications in practical situation. Transformation methods can be used to generate the non-Gaussian random surface [17]. The Gaussian random surface can be generated easily by the spectral method, which is widely used in the calculation of wave scattering [18]. The power spectral density of rough surface is a function of the spatial frequency, and determines the power contained in the spatial Fourier components of the surface profile. For one-dimensional Gaussian rough surface, the Gaussian spectrum is given by [18]

$$f(x) = \frac{1}{L} \sum_{n=-N/2}^{N/2-1} F(K_n) \exp(iK_n x) \tag{1}$$

where $F(K_n) = \sqrt{2\pi L W(K_n)} \left\{ \begin{array}{ll} \frac{N(0,1)+iN(0,1)}{\sqrt{2}}, & n \neq 0, \frac{N}{2} \\ N(0,1), & n = 0, \frac{N}{2} \end{array} \right\}$, L is the length of realization. For $n < 0$, $F(K_n) = F^*(-K_{-n})$, where the asterisk implies complex conjugate. $N(0,1)$ is a random variant with

a Gaussian distribution of zero mean and unit variance. $K_n = 2\pi n/L$, $i = \sqrt{-1}$, and $W(k) = \frac{h^2 l}{\sqrt{4\pi}} \exp(-\frac{k^2 l^2}{4})$ is the Gaussian spectrum amplitude density function. l is the correlation length in the x direction, h is the root mean square (rms) height of the rough surface, and k is the spatial frequency in the x direction.

3. ELECTROMAGNETIC SCATTERING FROM TARGETS LOCATED ABOVE OR BELOW A ROUGH SURFACE (VERTICAL POLARIZATION OR TM CASE)

To avoid artificial edge diffraction, the incident field should not be expressed as a plane wave, but instead contains a narrow angular distribution of energy about the mean incident grazing angle. The tapered plane wave developed by Thorsos [18] satisfied this requirement, and was chosen as the incident field. This incident wave satisfied the Maxwell's equations in an approximate sense. Consider a tapered plane wave with time dependence $\exp(-i\omega t)$ incident on the 1-D rough surface with height profile function given by $z = Z(x)$. The incident tapered plane wave can be expressed as

$$\psi^{in}(\mathbf{r}) = \exp[ik_0(x\sin\theta_i - z\cos\theta_i)(1 + w(\mathbf{r}))] \times \exp[-(x + z\tan\theta_i)^2/g^2] \tag{2}$$

where $w(\mathbf{r}) = [2(x + z\tan\theta_i)^2/g^2 - 1]/(k_0 g\cos\theta_i)^2$, θ_i is the incident angle defined with respect to the normal in the counterclockwise direction, g is the tapering parameter with the dimension of length and controls the tapering of the incident wave. Typically, if MoM is applied to a domain of length L, g is chosen to be some fraction of L. This paper uses $g = L/4$ to avoid artificial edge diffraction by tapering the incident field to zero for region exterior to the domain. The presence of $w(\mathbf{r})$ the term in (2) ensures that ψ^{in} satisfies the wave equation to the order of $1/(k_0 g\cos\theta_i)^2$, where $k_0 g\cos\theta_i \gg 1$ [18].

3.1. Formulation for EM Scattering from Targets Located above a Rough Surface

We assume that a PEC target is located above the rough surface shown in Fig. 1. Let $\psi_0(\mathbf{r})$ and $\psi_1(\mathbf{r})$ be the magnetic field in region 0 and region 1, respectively. The fields in region 0 and region 1 satisfy the following equations:

$$\frac{1}{2}\psi_0(\mathbf{r}) = \psi^{in}(\mathbf{r}) + \int_{s_r}\left[\psi_0(\mathbf{r}')\frac{\partial G_0(\mathbf{r}, \mathbf{r}')}{\partial n'} - G_0(\mathbf{r}, \mathbf{r}')\frac{\partial \psi_0(\mathbf{r}')}{\partial n'}\right]ds'$$
$$+ \int_{s_o}\psi_1(\mathbf{r}')\frac{\partial G_0(\mathbf{r}, \mathbf{r}')}{\partial n'}ds', \qquad \mathbf{r} \in s_r \text{ or } s_o \tag{3}$$
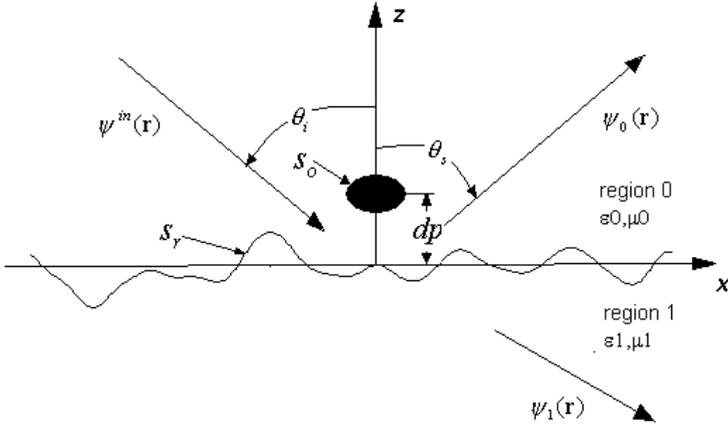
Figure 1. The geometry of a target situated above a rough surface.

$$\frac{1}{2}\psi_1(\mathbf{r}) = -\int_{s_r}\left[\psi_0(\mathbf{r}')\frac{\partial G_1(\mathbf{r},\mathbf{r}')}{\partial n'} - G_1(\mathbf{r},\mathbf{r}')\frac{\partial \psi_1(\mathbf{r}')}{\partial n'}\right]ds', \quad \mathbf{r}\in s_r \ (4)$$

Note that ψ^{in} is the incident field, $G_0(\mathbf{r},\mathbf{r}')$ and $G_1(\mathbf{r},\mathbf{r}')$ are the Green's functions for region 0 and region 1, where $G_0(\vec{r},\vec{r}') = (\frac{i}{4})H_0^{(1)}(k_0|\vec{r}-\vec{r}'|)$, $G_1(\vec{r},\vec{r}') = (\frac{i}{4})H_0^{(1)}(k_1|\vec{r}-\vec{r}'|)$, respectively, $H_0^{(1)}(\cdot)$ is zeroth-order Hankel function of the first kind. When $\mathbf{r}$ is on the rough surface ($\mathbf{r}\in s_r$), the field $\psi_0(\mathbf{r})$ and $\psi_1(\mathbf{r})$ satisfied the following equation based on boundary condition:

$$\psi_0(\mathbf{r})_{\mathbf{r}\in r_s} = \psi_1(\mathbf{r})|_{\mathbf{r}\in r_s} \tag{5}$$

$$\frac{\partial \psi_0(\mathbf{r})}{\partial n}\bigg|_{\mathbf{r}\in r_s} = \frac{1}{\rho}\frac{\partial \psi_1(\mathbf{r})}{\partial n}\bigg|_{\mathbf{r}\in r_s} \tag{6}$$

where $\rho = \varepsilon_1/\varepsilon_0$. The normal gradient of the 2-D Green's function is given by

$$\frac{\partial G(\mathbf{r},\mathbf{r}')}{\partial n'} = \frac{ik}{4}\hat{\mathbf{n}}\cdot\frac{\mathbf{r}-\mathbf{r}'}{|\mathbf{r}-\mathbf{r}'|}H_1^{(1)}(k|\mathbf{r}-\mathbf{r}'|) \tag{7}$$

where $\hat{\mathbf{n}} = \frac{-Z'(x')\hat{x}+\hat{z}}{\sqrt{1+[Z'(x')]^2}}$. The rough surface s_r is discretized along the x-axis. The target's surface s_o is also discretized, and the MoM with point-matching is used. We can obtain the matrix equation from (3)–(4) as follows:

$$\begin{bmatrix} A & B & C \\ D & -\rho E & 0 \\ F & G & H \end{bmatrix}\begin{bmatrix} V_1 \\ V_2 \\ V_3 \end{bmatrix} = \begin{bmatrix} \psi^{in} \\ 0 \\ \psi^{in} \end{bmatrix} \tag{8}$$

where $V_1(x) = \psi_0(\vec{r})|_{\vec{r} \in s_r}$, $V_2(x) = \partial \psi_0 / \partial n|_{x \in s_r}$, $V_3(x) = \psi_0|_{x \in s_o}$. The elements of the matrix are shown below:

$$A_{mn} = \begin{cases} -\gamma_n \Delta x \dfrac{ik_0}{4} (\mathbf{n} \cdot \mathbf{R}) H_1^{(1)}(k_0 |\mathbf{r}_m - \mathbf{r}_n|), & m \neq n \\[2mm] \dfrac{1}{2} - \dfrac{Z''(x_m) \Delta x}{4\pi \gamma_m^2}, & m = n \end{cases} \tag{9a}$$

$$B_{mn} = \begin{cases} \gamma_n \Delta x \dfrac{i}{4} H_0^{(1)}(k_0 |\mathbf{r}_m - \mathbf{r}_n|), & m \neq n \\[2mm] \gamma_m \Delta x \dfrac{i}{4} H_0^{(1)}[k_0 \Delta x \gamma_m / (2e)], & m = n \end{cases} \tag{9b}$$

$$D_{mn} = \begin{cases} \gamma_n \Delta x \dfrac{ik_1}{4} (\mathbf{n} \cdot \mathbf{R}) H_1^{(1)}(k_1 |\mathbf{r}_m - \mathbf{r}_n|), & m \neq n \\[2mm] \dfrac{1}{2} + \dfrac{Z''(x_m) \Delta x}{4\pi \gamma_m^2}, & m = n \end{cases} \tag{9c}$$

$$E_{mn} = \begin{cases} \gamma_n \Delta x \dfrac{i}{4} H_0^{(1)}(k_1 |\mathbf{r}_m - \mathbf{r}_n|), & m \neq n \\[2mm] \gamma_m \Delta x \dfrac{i}{4} H_0^{(1)}[k_1 \Delta x \gamma_m / (2e)], & m = n \end{cases} \tag{9d}$$

where $\mathbf{n} = \dfrac{-Z'(x_n)\hat{x} + \hat{z}}{\sqrt{1 + [Z'(x_n)]^2}}$, $\mathbf{R} = \dfrac{\mathbf{r}_m - \mathbf{r}_n}{|\mathbf{r}_m - \mathbf{r}_n|}$, $\gamma_n = \sqrt{1 + [Z'(x_n)]^2}$. k_0 is the wave-number in free space, $k_1 = \omega \sqrt{\mu_1 \varepsilon_1}$, $\gamma_m = \sqrt{1 + [Z'(x_m)]^2}$, $e = 2.71828138$, $Z'(x_m)$ and $Z''(x_m)$ are the first-order differential, the second-order differential of rough surface height function. We can obtain the impedance terms C, F, G and H of the matrix as follows:

$$C_{mp} = -\gamma_{op} \Delta x \frac{ik_0}{4} (\mathbf{n}_o \cdot \mathbf{R}_1) H_1^{(1)}(k_0 |\mathbf{r}_m - \mathbf{r}_{op}|) \tag{10a}$$

$$F_{qn} = -\gamma_n \Delta x \frac{ik_0}{4} (\mathbf{n} \cdot \mathbf{R}_2) H_1^{(1)}(k_0 |\mathbf{r}_{oq} - \mathbf{r}_n|) \tag{10b}$$

$$G_{qn} = \gamma_n \Delta x \frac{i}{4} H_0^{(1)}(k_0 |\mathbf{r}_{oq} - \mathbf{r}_n|) \tag{10c}$$

$$H_{qp} = \begin{cases} -\gamma_{op} \Delta x \dfrac{ik_0}{4} (\mathbf{n}_o \cdot \mathbf{R}_3) H_1^{(1)}(k_0 |\mathbf{r}_{oq} - \mathbf{r}_{op}|), & q \neq p \\[2mm] \dfrac{1}{2} - \dfrac{Z_0''(x_i) \Delta x}{4\pi \gamma_{op}^2}, & q = p \end{cases} \tag{10d}$$

where $\mathbf{n}_o = \dfrac{-Z_o'(x_{op})\hat{x} + \hat{z}}{\sqrt{1 + [Z_o'(x_{op})]^2}}$, $\mathbf{R}_1 = \dfrac{\mathbf{r}_m - \mathbf{r}_{op}}{|\mathbf{r}_m - \mathbf{r}_{op}|}$, $\gamma_{op} = \sqrt{1 + [Z_o'(x_{op})]^2}$, $\mathbf{R}_2 = \dfrac{\mathbf{r}_{oq} - \mathbf{r}_n}{|\mathbf{r}_{oq} - \mathbf{r}_n|}$ and $\mathbf{R}_3 = \dfrac{\mathbf{r}_{oq} - \mathbf{r}_{op}}{|\mathbf{r}_{oq} - \mathbf{r}_{op}|}$.

Upon solving the matrix equation (8), the scattering field in region 0 is given by

$$\psi_s(\vec{r}) = \frac{e^{ikr}}{\sqrt{r}}\psi_s^N(\theta_s, \theta_i) \tag{11a}$$

where

$$\psi_s^N(\theta_s, \theta_i) = \frac{i}{4}\sqrt{\frac{2}{\pi k_0}}e^{-i\pi/4}$$

$$\cdot \left\{ \int_{s_r}[-i(\mathbf{n}\cdot\mathbf{k}_s)V_1(x) - V_2(x)]\exp(-i\mathbf{k}_s\cdot\mathbf{r})\sqrt{1+[Z'(x)]^2}dx \right.$$

$$\left. - \int_{s_o}i(\mathbf{n}_o\cdot\mathbf{k}_s)V_3(x)\exp(-i\mathbf{k}_s\cdot\mathbf{r})\sqrt{1+[Z_o'(x)]^2}dx \right\} \tag{11b}$$

with $\mathbf{k}_s = k_0(\sin\theta_s\hat{x} + \cos\theta_s\hat{z})$.

The expression for the normalized scattering coefficient with tapered plane wave incidence is given by [19]

$$\sigma_V(\theta_s) = \frac{|\psi_s(\theta_s, \theta_i)|^2}{g\sqrt{\pi/2}\cos\theta_i\left(1 - \dfrac{1 + 2\tan^2\theta_i}{2k_0^2g^2\cos^2\theta_i}\right)}. \tag{11c}$$

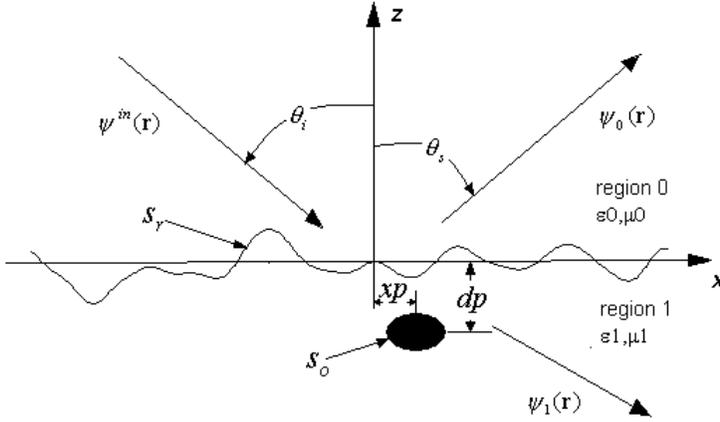## 3.2. Formulation for EM Scattering from Targets Located below a Rough Surface

The scattered field from a PEC target buried below a rough surface can be obtained using the same method described above. The geometry of the problem is shown in Fig. 2. The incident field, scattered field and transmitted field satisfied the following equations on the rough surface and the surface of the target, as follows

$$\frac{1}{2}\psi_0(\mathbf{r}) = \psi^{in}(\mathbf{r}) + \int_{s_r}\left[\psi_0(\mathbf{r}')\frac{\partial G_0(\mathbf{r}, \mathbf{r}')}{\partial n'} - G_0(\mathbf{r}, \mathbf{r}')\frac{\partial\psi_0(\mathbf{r}')}{\partial n'}\right]ds',$$
$$\mathbf{r} \in s_r; \quad (12a)$$

$$\frac{1}{2}\psi_1(\mathbf{r}) = -\int_{s_r}\left[\psi_1(\mathbf{r}')\frac{\partial G_1(\mathbf{r}, \mathbf{r}')}{\partial n'} - G_1(\mathbf{r}, \mathbf{r}')\frac{\partial\psi_1(\mathbf{r}')}{\partial n'}\right]ds'$$
$$- \int_{s_o}\psi_1(\mathbf{r}')\frac{\partial G_1(\mathbf{r}, \mathbf{r}')}{\partial n'}ds', \quad\quad \mathbf{r} \in s_r; \quad (12b)$$

$$\frac{1}{2}\psi_1(\mathbf{r}) = -\int_{s_r}\left[\psi_1(\mathbf{r}')\frac{\partial G_1(\mathbf{r}, \mathbf{r}')}{\partial n'} - G_1(\mathbf{r}, \mathbf{r}')\frac{\partial\psi_1(\mathbf{r}')}{\partial n'}\right]ds'$$
$$- \int_{s_o}\psi_1(\mathbf{r}')\frac{\partial G_1(\mathbf{r}, \mathbf{r}')}{\partial n'}ds', \quad\quad \mathbf{r} \in s_o. \quad (12c)$$

Figure 2. The geometry of a target situated below a rough surface.

Using the boundary condition, $\psi_0(\mathbf{r})_{\mathbf{r}\in r_s} = \psi_1(\mathbf{r})|_{\mathbf{r}\in r_s}$, $\frac{\partial\psi_0(\mathbf{r})}{\partial n}|_{\mathbf{r}\in r_s} = \frac{1}{\rho}\frac{\partial\psi_1(\mathbf{r})}{\partial n}|_{\mathbf{r}\in r_s}$ and the same discretisation procedure as in Section 3.1, we obtain the following matrix equation:

$$
\begin{bmatrix} A & B & 0 \\ C & -\rho D & E \\ F & -\rho G & H \end{bmatrix} \begin{bmatrix} V_1 \\ V_2 \\ V_3 \end{bmatrix} = \begin{bmatrix} \psi^{in} \\ 0 \\ 0 \end{bmatrix} \tag{13}
$$

where $V_1(x) = \psi_0(\vec{r})|_{\vec{r}\in s_r}$, $V_2(x) = \partial\psi_0/\partial n|_{x\in s_r}$, $V_3(x) = \psi_1|_{x\in s_o}$ and $\rho = \varepsilon_1/\varepsilon_0$. The elements in above equation can be expressed as

$$
A_{mn} = \begin{cases} -\gamma_n\Delta x\dfrac{ik_0}{4}(\mathbf{n}\cdot\mathbf{R})H_1^{(1)}(k_0|\mathbf{r}_m - \mathbf{r}_n|), & m \neq n \\[2mm] \dfrac{1}{2} - \dfrac{Z''(x_m)\Delta x}{4\pi\gamma_m^2}, & m = n \end{cases} \tag{14a}
$$

$$
B_{mn} = \begin{cases} \gamma_n\Delta x\dfrac{i}{4}H_0^{(1)}(k_0|\mathbf{r}_m - \mathbf{r}_n|), & m \neq n \\[2mm] \gamma_m\Delta x\dfrac{i}{4}H_0^{(1)}[k_0\Delta x\gamma_m/(2e)], & m = n \end{cases} \tag{14b}
$$

$$
C_{mn} = \begin{cases} \gamma_n\Delta x\dfrac{ik_1}{4}(\mathbf{n}\cdot\mathbf{R})H_1^{(1)}(k_1|\mathbf{r}_m - \mathbf{r}_n|), & m \neq n \\[2mm] \dfrac{1}{2} + \dfrac{Z''(x_m)\Delta x}{4\pi\gamma_m^2}, & m = n \end{cases} \tag{14c}
$$

$$
D_{mn} = \begin{cases} \gamma_n \Delta x \dfrac{i}{4} H_0^{(1)}(k_1|\mathbf{r}_m - \mathbf{r}_n|), & m \neq n \\[2mm] \gamma_m \Delta x \dfrac{i}{4} H_0^{(1)}[k_1 \Delta x \gamma_m/(2e)], & m = n \end{cases} \tag{14d}
$$

$$
E_{mp} = \gamma_{op} \Delta x \frac{ik_1}{4}(\mathbf{n}_o \cdot \mathbf{R}_1) H_1^{(1)}(k_1|\mathbf{r}_m - \mathbf{r}_{op}|) \tag{15a}
$$

$$
F_{qn} = \gamma_n \Delta x \frac{ik_1}{4}(\mathbf{n} \cdot \mathbf{R}_2) H_1^{(1)}(k_1|\mathbf{r}_{oq} - \mathbf{r}_n|) \tag{15b}
$$

$$
C_{qn} = -\gamma_n \Delta x \frac{i}{4} H_0^{(1)}(k_1|\mathbf{r}_{oq} - \mathbf{r}_n|) \tag{15c}
$$

$$
H_{qp} = \begin{cases} \gamma_{op} \Delta x \dfrac{ik_1}{4}(\mathbf{n}_o \cdot \mathbf{R}_3) H_1^{(1)}(k_1|\mathbf{r}_{oq} - \mathbf{r}_{op}|), & q \neq p \\[3mm] \dfrac{1}{2} + \dfrac{Z_o''(x_{op})\Delta x}{4\pi\gamma_{op}^2}, & q = p \end{cases} \tag{15d}
$$

where the expressions for $\mathbf{n}, \mathbf{R}, \gamma_n, \mathbf{n}_o, \mathbf{R}_1, \mathbf{R}_2, \mathbf{R}_3$ and γ_{op} are given in Section 3.1. $Z_o''(x_{op})$ is the second-order derivative of the target's surface function at the point x_{op}. In the above equation, $m, n = 1, 2, \ldots, N$, $p, q = 1, 2, \ldots, N_o$, where N is the number of discretisation points on the rough surface, N_o is number of discretisation points on the object's surface. $Z(x)$ is the profile of the rough surface, and $Z_o(x)$ is the profile function of the object's surface.

Upon calculating the unknown surface currents $V_1(x)$ and $V_2(x)$ using MoM, the scattered field at any point above the rough surface can be obtained by integrating the product of the surface current with the Green's function. The scattered field in the region 0 is given by

$$
\psi_s(\vec{r}) = \frac{e^{ikr}}{\sqrt{r}} \psi_s^N(\theta_s, \theta_i) \tag{16a}
$$

where

$$
\psi_s^N(\theta_s, \theta_i) = \frac{i}{4}\sqrt{\frac{2}{\pi k_0}} e^{-i\pi/4}
$$
$$
\int_{s_r} [-i(\mathbf{n} \cdot \mathbf{k}_s)V_1(x) - V_2(x)] \exp(-i\mathbf{k}_s \cdot \mathbf{r})\sqrt{1 + [Z'(x)]^2} dx. \tag{16b}
$$

The normalized scattering cross section for tapered plane wave

incidence is given by [19]

$$\sigma_H(\theta_s) = \frac{|\psi_s(\theta_s, \theta_i)|^2}{g\sqrt{\pi/2}\cos\theta_i\left(1 - \dfrac{1 + 2\tan^2\theta_i}{2k_0^2 g^2 \cos^2\theta_i}\right)}. \qquad (16c)$$

4. DETECTION OF TARGETS BELOW A ROUGH SURFACE

Consider the incident fields at the two directions θ_{i1}, θ_{i2}, and the corresponding scattered fields at θ_{s1} and θ_{s2}, respectively. The ACF is given by Eq. (17) below. The ACF can be calculated based on realization averaging. The ensemble average is obtained by taking the average over different samples (rough surface scatterers) with the same statistics.

$$\Gamma(\theta_{s1}, \theta_{i1}, \theta_{s2}, \theta_{i2}) = \langle \psi_s(\theta_{s1}, \theta_{i1}) \cdot \psi_s^*(\theta_{s2}, \theta_{i2}) \rangle / \sqrt{W_1 W_2}$$

$$= \frac{1}{N_r}\sum_{q=1}^{N_r} \psi_s(\theta_{s1}, \theta_{i1}, q) \cdot \psi_s^*(\theta_{s2}, \theta_{i2}, q)/\sqrt{W_1 W_2} \quad (17)$$

where q is the realization index; N_r is the number of realizations, and W_1, W_2 are the energy fluxes through the surface at incident angles θ_{i1} and θ_{i2}, respectively. These are given by

$$W_1 = \sqrt{\frac{\pi}{2}}g\cos\theta_{i1}\left(1 - \frac{1 + 2\tan^2\theta_{i1}}{2k_0^2 g^2 \cos^2\theta_{i1}}\right),$$

$$W_2 = \sqrt{\frac{\pi}{2}}g\cos\theta_{i2}\left(1 - \frac{1 + 2\tan^2\theta_{i2}}{2k_0^2 g^2 \cos^2\theta_{i2}}\right).$$

5. ANALYSIS ON THE STATISTICAL CHARACTERISTICS OF THE COMPOSITE SCATTERED FIELD

When a target is located on land or sea and illuminated by radar, the object echoes are superimposed upon the return of the land or sea. The undesired echoes are known as clutter in radar terminology. The statistical characteristics of clutter will depend on several parameters, namely the incident angle, transmitted frequency, spatial resolution, sea state, wind direction and intensity. The polarization also affects the statistical character of clutter, particularly for grazing angles less than $20°$. Nevertheless, for the purpose of target detection, it is

sometime necessary to have the probability density function (PDF) of the amplitude and correlation property of the sea or land backscattered signal. Therefore, the statistical models proposed in the literature mainly consist of stochastic processes with different clutter amplitude, distribution (such as Rayleigh, Weibull, Log-normal, K distribution etc). For completeness, we repeat the expressions of these PDFs below:

A. Rayleigh distribution

$$\text{PDF}: \qquad p(x) = \frac{2x}{a} \exp(x^2/a), \qquad x \geq 0 \qquad (18)$$

The characteristic parameters of the Rayleigh are estimated by using the method of moment [20], i.e., $a = 4 \langle x \rangle^2 / \pi$.

B. Weibull distribution

$$\text{PDF}: \qquad p(x) = n \left[\frac{x^{n-1}}{a} \right] \exp\left[-\frac{x^n}{a} \right], \qquad x > 0 \qquad (19)$$

The cumulative probability density function is given by $F(x) = 1 - \exp(-x^n/a)$, where n is the shape parameter and a is the scale parameter. When $n = 2$, the Weibull distribution becomes the Rayleigh distribution. The characteristic parameter can be obtained by fitting the function of $\ln[-\ln(1 - F)] = n \ln x - \ln a$, in the least square sense.

C. Log-normal distribution

$$\text{PDF}: \qquad p(x) = \exp\left\{ -(\ln x - m)^2/a \right\} / \left(x\sqrt{\pi a} \right) \qquad (20)$$

where m, a, are the characteristic parameters. The characteristic parameters are obtained using the method of moment, and are given by $a = 2(\ln x_2 - 2 \ln x_1)$, $m = \ln x_1 - \frac{a}{4}$, $x_1 = \langle x \rangle = \exp(m + \frac{a}{4})$ and $x_2 = \langle x^2 \rangle = \exp(2m + a)$, where $\langle x^n \rangle$ represents the nth order moment.

## 6. NUMERICAL RESULTS AND DISCUSSIONS

6.1. Validation and Efficiency of the Computations

Reference [25] presents a rigorous analysis of the plane-wave scattering from a perfectly electrically conducting (PEC) circular cylinder in front of a reflecting surface by cylindrical-wave approach and imposing the electromagnetic boundary conditions on the surface of the conducting cylinder. The scattering of a Gaussian beam by a PEC cylinder placed
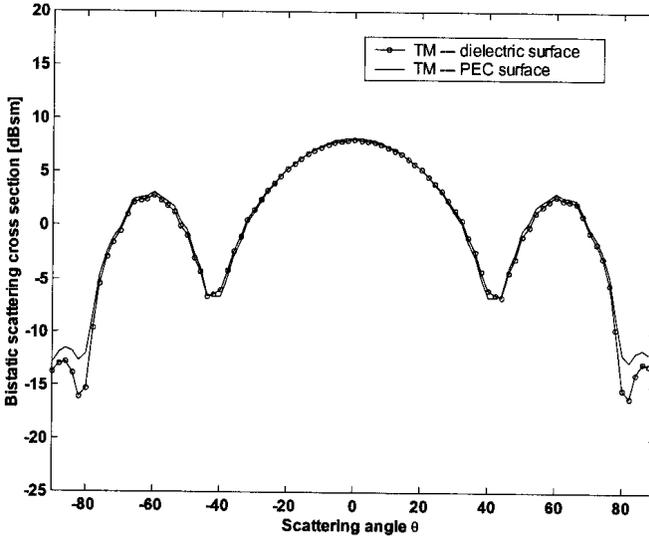
Figure 3. Bistatic scattering cross section versus the scattering angle for a PEC cylinder of diameter 1.2732λ on a flat substrate for incidence angle $\theta_i = 0°$.
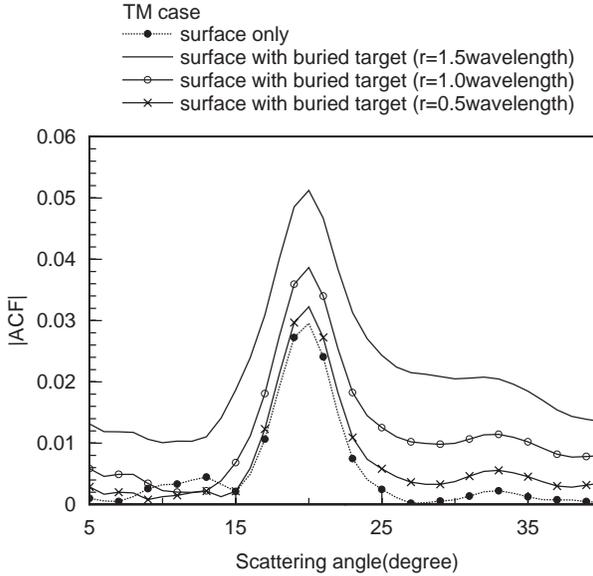
onto a conducting plane is carried out by means of the extinction theorem [26]. Hence, the validation and efficiency of the computations is checked by comparisons with results obtained from reference [26] using the Gaussian beam as incident wave for planar surface. The axis of PEC the cylinder of diameter 1.2732λ is along the $\hat{y}$ direction. Results are shown in Figure 3 for PEC and dielectric planar surface as substrate respectively, the incidence angle is $\theta_i == 0°$ and scattering angles is $\theta_s = -90° \sim 90°$. The dielectric half space is characterized by the relative permittivity $\varepsilon_r = 250$, which has a strong reflection. This case may be useful for comparison with the results in the presence of the PEC planar surface. The incidence wave is tapered with the tapering parameter $g = L/4$, where the length of the rough surface is $L = 20\lambda$ for the planar surface. Our results are in excellent agreement with that reported in [26]. The results are identical except for the presence of a central peak that is due to the reflection of the incident Gaussian beam by the planar surface, which is not shown in our figures. The ground surface and the targets are discretized into $N = 512$ and $N_0 = 60$ points, respectively.
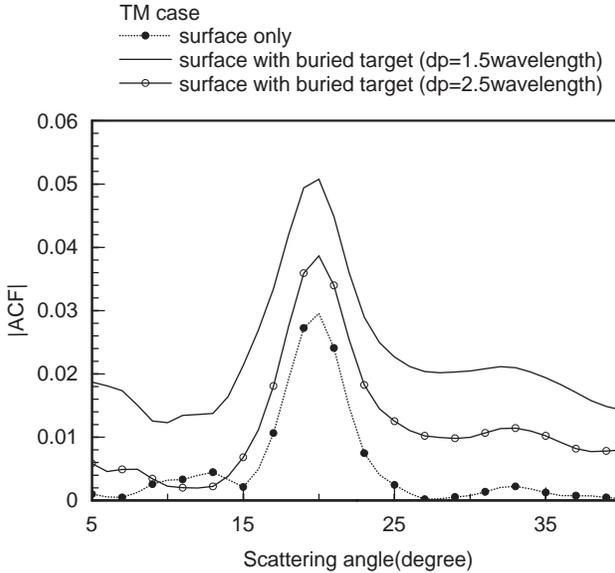
Figure 4. ACF at backscattering direction for two different depth of buried target.

6.2. Discussions

The potential application of the ACF to detect buried target can be seen by comparing the ACF with realization averaging of the wave scattered by rough surface only and that of the rough surface with buried target. Over 150 realizations of the rough surfaces are considered. The difference in the ACF with and without the object below the rough surface, especially in the backscattering direction, is significant. Numerical results are shown for monostatic scattering at $\theta_{i1} = -\theta_{s1} = 20°$, with varying θ_{i2} and θ_{s2} ($\theta_{s2} = -\theta_{i2}$). In our simulations, we have chosen a rough surface length of $L = 20\lambda$, the tapering parameter $g = L/4$, with the frequency at $1.2\,\text{GHz}$. Fig. 4 shows the amplitudes of the ACF for the same target at two different depths. The radius of circular cylinder is $r = 1.0\lambda$. The other parameters used are: $h = 0.25\lambda$, $l = 0.5\lambda$, $\varepsilon_{1r} = (3.7, 0.13)$ and $xp = 0$. It is observed that the amplitude of the ACF decreases with increasing depth, but both are higher than that of the rough surface scattering without the buried target at certain scattering angles. The number of discretisation points on the rough surface and the surface of the target are $N_r = 512$ and $N_o = 100$, respectively. The size of matrices in calculation are 1124×1124. The effect of the depth of the target

TM case
·······●······· surface only
————— surface with buried target (r=1.5wavelength)
——○—— surface with buried target (r=1.0wavelength)
——×—— surface with buried target (r=0.5wavelength)

Figure 5. ACF at backscattering direction for three different buried target size.

on the electromagnetic scattering of buried target below rough surface interface depend on the rms surface height, surface correlation length type of roughness spectrum, polarization of incident field, beamwidth, incidence angle, and soil characteristic. Thus, it should be noted that the results presented in the paper apply only to the particular case, here the limitation on the distance d_p given a certain value. Fig. 5 shows the amplitude of the ACF for buried targets of three different sizes, with $r = 0.5\lambda$, $r = 1.0\lambda$ and $r = 1.5\lambda$. The other parameters used are: $h = 0.25\lambda$, $l = 0.5\lambda$, $xp = 0\lambda$, $dp = 2.5\lambda$ and $\varepsilon_{1r} = (3.7, 0.13)$. The results showed that the amplitude of the ACF decreases as the size of target decreases. The amplitude of the ACF, as a function of the horizontal position of the buried target, is shown in Fig. 6. The other parameters are given by $h = 0.25\lambda$, $l = 0.5\lambda$, $r = 1.5\lambda$, $dp = 2.5\lambda$ and $\varepsilon_{1r} = (3.7, 0.13)$. When the buried target is within the incident beam, the scattered field consists of the scattering from both the buried target and the rough surface. The amplitude of the ACF with buried target is larger than that of the rough surface without target (horizontal position x_p is less than about 2.0λ). On the other hand, when the horizontal position x_p is greater than 4.0λ, the amplitude of the ACF is comparable to that of the rough surface scattering only, since the
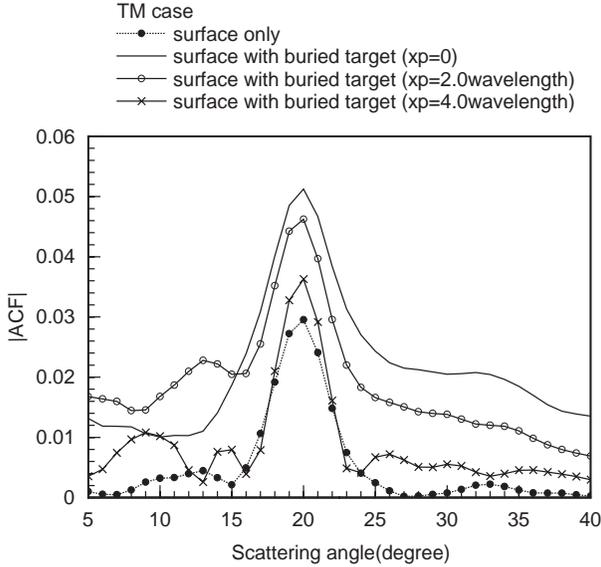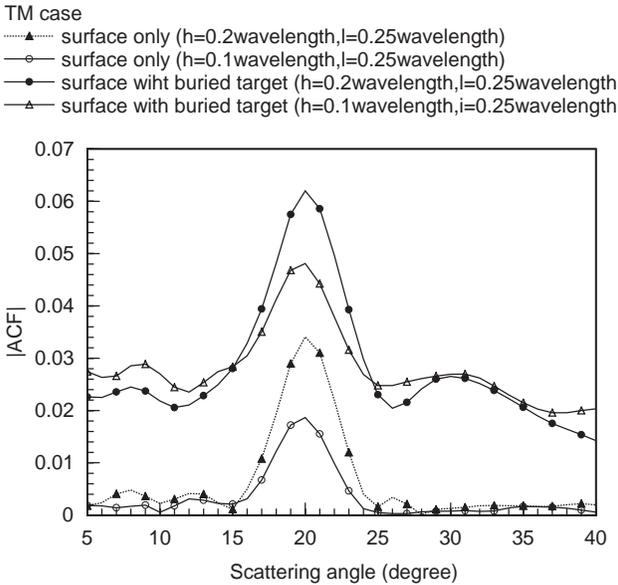
Figure 6. ACF at backscattering direction for different horizontal position of the buried target.

buried target is not located within the incident wave beamwidth. The results on the amplitude of the ACF for different water content in the soil are given in Fig. 7. The other parameters used are given by $h = 0.25\lambda$, $l = 0.5\lambda$, $r = 1.0\lambda$, $xp = 0$ and $dp = 1.5\lambda$. The relative permittivity values $\varepsilon_{1r} = (3.7, 0.13)$ and $\varepsilon_{1r} = (16.76, 1.15)$ corresponded to the case of soil with water content of 5% and 30% (in region 1). Fig. 7 shows that the amplitude of the ACF for scattering from surface with buried target is comparable to that of the scattering from rough surface, due to the large attenuation of wave propagating in the soil with 30% water content. Fig. 8 shows the ACF at backscattering direction for different rough surface properties. The other parameters used are: $r = 1.0\lambda$, $xp = 0$, $dp = 1.5\lambda$ and $\varepsilon_{1r} = (3.7, 0.13)$. Results show that the amplitudes of the ACF for two different root-mean-square heights are similar. The peak at the scattering angle 20 degrees for Figure 4 to 8 can be explained as follows: Numerical results shown in Figure 4 to 8 are for reference angles at $\theta_{i1} = -\theta_{s1} = 20°$. with varying θ_{i2} and θ_{s2} ($\theta_{s2} = -\theta_{i2}$). This configuration provides the backscattering cross section, but the ACF magnitude intercept the memory line at $\theta_{s2} = 20°$ on which the phase matching condition occurs. Thus, the peak can be observed. In general, the backscattering cross section varies slowly as a function of
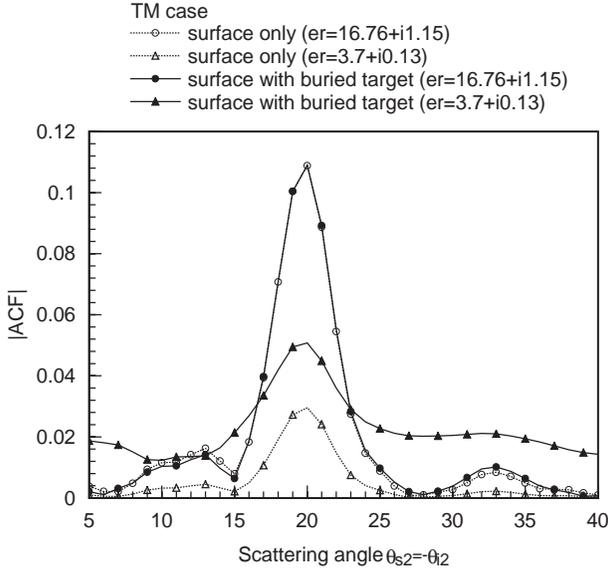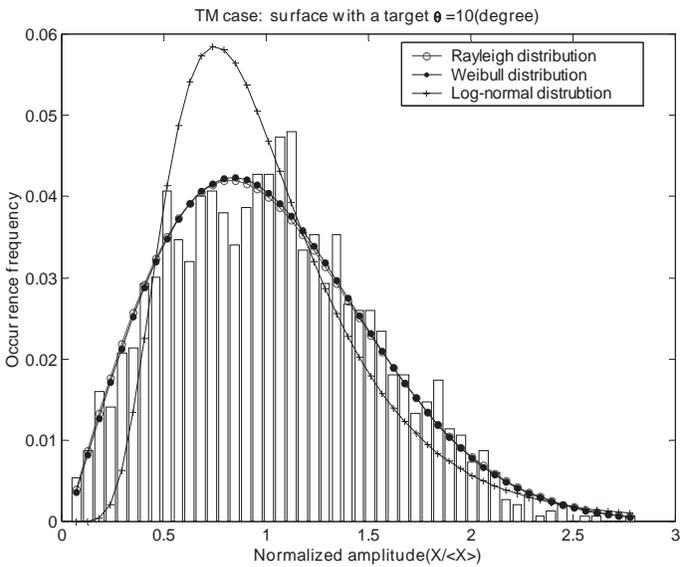
Figure 7. ACF at backscattering direction for soil with different water content.

Figure 8. ACF at backscattering direction for different rough surface properties.
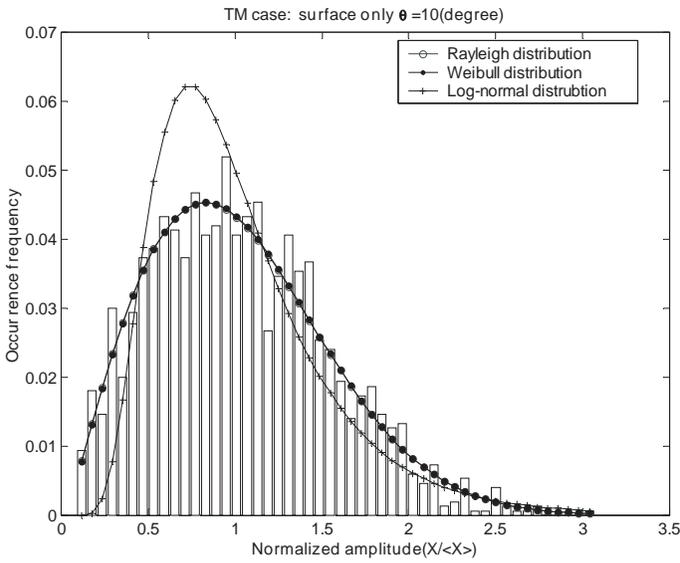
Figure 9a. Amplitude histogram for surface only (TM case).

Figure 9b. Amplitude histogram for surface with a target (TM case).

Table 1. Estimated model parameter for incident angle of 10 (degree) (TM case).

TM case	Shape parameter		Scale parameter	
	Surface only	Surface with target	Surface only	Surface with target
Rayleigh	$c = 2$	$c = 2$	$a = 1.2732$	$a = 1.2732$
Weibull	$n = 2.0066$	$n = 2.0288$	$a = 1.2761$	$a = 1.2801$
Log-normal	$m = -0.1154$	$m = -0.1095$	$a = 0.4615$	$a = 0.4379$

angle, whereas the ACF decrease small away from the memory line due to the destructive phase interface in the coherent averaging process.

Finally, statistical analysis for the amplitude of the composite scattered field from target located above rough surface was performed on about 1500 samples. We compared the empirical distribution estimated from the data (or histogram) with Rayleigh, Weibull and Log-normal distribution. The results of this histogram analysis are shown in Fig. 9, and the value of the characteristic parameters is summarized in Table 1. It is noted that the simulated data is very close to the Rayleigh distribution for the amplitude of the composite scattered field from rough surface only and from surface with target, in the TM case. The Weibull distribution with $n = 2.0066$ can be approximated by the Rayleigh distribution. The worst fitting is shown by the Log-normal distribution, as the Log-normal distribution occurred mainly in high resolution radar for low grazing angles. The parameters used in the calculation are: frequency $= 1.2\,\text{GHz}$, $\theta_s = -\theta_i$; rough surface parameter: $h = 0.25\lambda$, $l = 0.5\lambda$, $L = 40\lambda$ and $g = L/4$; circular cylindrical target parameter: $r = 1.0\lambda$, $xp = 0$, and $dp = 1.5\lambda$.

7. CONCLUSIONS

Using the point-matching method with pulse basis functions, the scattered field from random rough surface and the composite scattered field from a target placed over or below the rough surface for TM incidence can be solved numerically. The simulation results show that the scattered field from both rough surface and target can broaden the angular correlation function, even at angles away from the memory line. The broadening of the ACF width can be used to detect buried target, since the rough surface scattering is suppressed and the buried target scattering become more conspicuous. The statistical properties of the composite scattered field amplitude can be approximated by the Rayleigh and Weibull distributions.

REFERENCES

1. Geng, N., M. A. Ressler, and L. Carin, "Wide-band VHF scattering from a trihedral reflector situated above a lossy dispersive half space," *IEEE Trans. Geosci. Remote Sensing*, Vol. GRS-37, No. 5, 2609–2617, 1999.

2. Cui, T. J. and W. C. Chew, "Fast algorithm for electromagnetic scattering by buried 3-D dielectric objects of large size," *IEEE Trans. Geosci. Remote Sensing*, Vol. GRS-37, No. 5, 2597–2608, 1999.

3. Zhang, Y., Y. E. Yang, H. Braunisch, and J. A. Kong, "Electromagnetic wave interaction of conducting object with rough surface by hybrid SPM/MOM technique," *PIERS 22: Progress in Electromagnetics Research*, Vol. 22, 315–335, 1999.

4. Chiu, T. and K. Sarabandi, "Electromagnetic scattering interaction between a dielectric cylinder and a slightly rough surface," *IEEE Trans. Antennas Propagat.*, Vol. AP-47, No. 5, 902–913, 1999.

5. Wang, X., X. Luo, Z. Zhang, and J. Fu, "The study of an electromagnetic scattering model for two adjacent trunks above a rough surface ground plane," *Microwave Opt. Tech. Lett.*, Vol. 20, No. 6, 369–376, 1999.

6. Wang, X., X. Luo, Z. Zhang, and J. Fu, "Electromagnetic scattering from target buried in layer of randomly distributed trunks," *Microwave Opt. Tech. Lett.*, Vol. 24, No. 3, 162–166, 2000.

7. Wang, X., Z. Zhang, and J. Fu, "Detection of targets buried in fractal trees by using the polarization angular correlation function," *Journal of Electromagnetic Waves and Applications*, Vol. 14, No. 7, 891–902, 2000

8. O'Neill, K., R. F. Lussky, and K. D. Paulsen, "Scattering from a metallic object embedded near the randomly rough surface of a lossy dielectric," *IEEE Trans. Geosci. Remote Sensing*, Vol. GRS-34, No. 2, 367–376, 1996.

9. Zhang, G., L. Tsang, and K. Pak, "Angular correlation function and scattering coefficient of electromagnetic waves scattered by a buried object under a two-dimensional rough surface," *J. Opt. Soc. Am. A*, Vol. 15, 2995–3002, 1998.

10. Peters, L., J. Daniels, and J. Young, "Ground penetrating radar as a subsurface environmental sensing tool," *Proc. IEEE*, Vol. 82, 1802–1822, 1994.

11. Feng, S., C. Kane, P. A. Lee, and A. D. Stone, "Correlations

and fluctuations of coherent wave transmission through disordered media," *Phys. Rev. Lett.*, Vol. 61, No. 7, 834–837, 1988

12. Michel, T. R. and K. A. O'Donnell, "Angular correlation functions of amplitudes scattered from a one-dimensional, perfectly conducting rough surface," *J. Opt. Soc. Am. A*, Vol. 9, No. 8, 1374–1384, 1992.

13. Tsang, L, G. Zhang, and K. Pak, "Detection of a buried object under a single random rough surface with angular correlation function in EM wave scattering," *Microwave Opt. Tech. Lett.*, Vol. 11, No. 6, 300–304, 1996.

14. Zhang, G. F., L. Tsang, and Y. Kuga, "Studies of the angular correlation function of scattering by random rough surfaces with and without a buried object," *IEEE Trans. Geosc. Remote Sensing*, Vol. GRS-35, No. 2, 444–453, 1997.

15. Goff, J. A., "A utilitarian approach to modeling non-Gaussian characteristics of a topographic field," *J. Geophys. Res.*, Vol. 98 (B11), No. 19, 635–647, 1993.

16. Tatarskii, V. I. and V. I. Tatarskii, "Non-Gaussian statistical model of the ocean surface for wave-scattering theories," *Waves Random Media*, Vol. 6, No. 4, 419–435, 1996.

17. Johnson, G. E., "Constructions of particular random process," *Proc. IEEE*, Vol. 82, No. 2, 270–284, 1994.

18. Thorsos, E., "The validity of the Kirchhoff approximation for rough surface scattering using a Gaussian roughness spectrum," *J. Acoust. Soc. Am.*, Vol. 83, No. 1, 78–92, 1988.

19. Donohue, D. J., H. C. Ku, and D. R. Thompson, "Application of iterative moment-method solution to ocean surface radar scattering," *IEEE Trans. Antennas Propagat.*, Vol. AP-46, No. 1, 121–132, 1998.

20. Kay, S. M., *Fundamentals of Statistical Signal Processing: Estimation Theory*, Prentice-Hall, Englewood Cliffs, NJ, 1993

21. Cottis, P. G., C. N. Vazouras, C. Kalamatianos, and J. D. Kanellopoulos, "Scattering of TM waves from a cylindrical scatterer buried inside a two-layer lossy ground with sinusoidal surface," *J. Electromagn. Waves Appl.*, Vol. 10, No. 7, 1005–1021, 1996.

22. Chiu, T. and K. Sarabandi, "Electromagnetic scattering interaction between a dielectric cylinder and a slightly rough surface," *IEEE Trans. Antennas Propagat.*, Vol. 47, No. 5, 902–913, 1999.

23. Johnson, J. T., "Thermal emission from a layered medium

bounded by a slightly rough interface," *IEEE Trans. Geosci. Remote Sensing*, Vol. 39, 368–378, 2001.

24. Fuks, M. and A. G. Voronovich, "Wave diffraction by rough interfaces in an arbitrary plane-layered medium," *Waves Random Media*, Vol. 10, 253–272, 2000.

25. Borghi, R., F. Frezza, F. Gori, M. Santarsiero, and G. Schettini, "Plane-wave scattering by a perfectly conducting circular cylinder near a plane surface: cylindrical-wave approach," *J. Opt. Soc. Am. A*, Vol. 13, No. 3, 483–493, 1996.

26. Valle, P. J., F. Gonzalez, and F. Moreno, "Electromagnetic wave scattering from conducting cylindrical structures on flat substrates: study by means of the extinction theorem," *Appl. Opt.*, Vol. 33, No. 3, 512–523, 1993.